Supplementary information

Dome-shaped Mode lasing from Liquid Crystal for Full-Color Laser and High-Sensitivity Detection

Rui Duan,[#a] *Zitong Zhang,*[#a] *Lian Xiao,*[a] *Tianhua Ren,*[a] *Xuehong Zhou,*[a] *Yi Tian Thung,*[a] *Van Duong Ta,**[b] *Jun Yang,**[c] *Handong Sun**[a]

[a] Division of Physics and Applied Physics, School of Physical and Mathematical Sciences, Nanyang Technological University, 637371, Singapore

[b] Department of Optical Devices, Le Quy Don Technical University, Hanoi 100000, Vietnam

[c] Guangdong Provincial Key Laboratory of Information Photonics Technology, College of Information Engineering, Guangdong University of Technology, Guangzhou 510006, China

[#] R. Duan and Z. T. Zhang contributed equally to this work.

* E-mail: duong.ta@lqdtu.edu.vn; yangj@gdut.edu.cn; HDSun@ntu.edu.sg

Contents

S1. Materials and methods

a. Cavity materials

Nematic liquid crystal 4′-Pentyl-4-biphenylcarbonitrile (5CB, 98%), which was purchased from Sigma-Aldrich, was selected as the cavity materials for the fabrication of high-quality DSM resonators due to its high refractive index and excellent flexibility.

b. Laser dyes

4-(dicyanomethylene)-2-methyl-6-(4-dimethylaminostyryl)-4H-pyran (DCM, 98%), Coumarin 504A (C504A), and 1,4-bis (2-methylstyryl)benzene (o-MSB), which have strong gains in red, green, and blue bands, were selected as the laser medium of the LC-DSM microlasers. The three laser dyes were purchased from Sigma-Aldrich, Exciton and Tokyo Chemical Industry, respectively. All selected laser dyes have good solubility in 5CB, which is conducive to the formation of low threshold and high-quality lasers.

c. Other materials

1H,1H,2H,2H-Perfluorooctyltriethoxysilane (PTES, 98%), which was purchased from Sigma-Aldrich, was selected as a hydrophobic material to be applied to the highly reflective distributed Bragg reflector (DBR) surface.

d. Substrate preparation

The DBR substrate was ultrasonically cleaned in acetone solution for 10 minutes to remove organic stains on the surface. The cleaned DBR substrate was blown dry using nitrogen gas for 5 minutes. A thin layer of PTES was coated on the surface of the DBR substrate.

e. Dye-doped LC materials preparation

Firstly, 0.005g laser dye was mixed with 1g 5CB LC, and then ultrasonic oscillation was carried out in a water bath at 45 ℃ for 30 minutes to ensure uniform mixing. The prepared LC cavity materials doped with different dyes are ready for use.

f. LC-DSM microlaser arrays preparation

Hemispherical LC-DSM microlasers were obtained by depositing dyes-doped LC materials on a prepared DBR hydrophobic substrate using a GIX^{TM} Microplotter^{TM} II

from Sonoplot, INC. The preparation process of the LC-DSM microlaser consists of first absorbing the dye-doped LC solution with a glass needle by capillary action, and then printing the microlaser monomers and designing laser arrays on the DBR substrate assisted by ultrasonic vibration. The size of the LC-DSM microcavities was controlled using glass needles with different tip diameters (Fig. S1).

g. Simulation

The electric field distributions of the DSM and WGM resonators were modelled by using the finite element method (commercial software COMSOL Multiphysics). In the Electromagnetic Waves, Frequency Domain (ewfd) of Wave optics in COMSOL Multiphysics, the 2D model was adopted for numerical simulation under Maxwell's boundary conditions. A perfectly matched layer (PML) and scattering boundary conditions are used as the external boundary of the model. The geometries of the droplet resonators were set to be parts of perfect rounds with different contact angles. A bottom-distributed Bragg reflector (DBR) was composed of 24 pairs dielectric layers alternating between high- refractive index (2.32) and low-refractive index (1.45) layers. The bottom diameter of the simulation model is set to 40 μm. The refractive indices of LCs and air are set as 1.71, and 1.0, respectively.

h. Lasing Measurement and Setup

The lasing behaviors of LC-DSM microlasers were characterized by a home-built micro-photoluminescence (μ-PL). The 532 nm and 355 nm Q-switched nanosecond Nd: YAG laser was selected as the excitation source. The laser was guided at an angle of about 45° to normal of the sample to pump the sample. Emission spectra were collected by an objective (50×, NA = 0.42), and delivered to a camera for a PL image or to silicon charge-coupled device (CCD) for recording spectra with a spectral resolution of ~0.02 nm. To investigate the polarization states of the lasing behaviors, a polarizer was placed orthogonally in the optical path between the sample emission and the spectrometer. At the fixed pump intensity, polarization characteristics were recorded as the dependence of emission intensity on the change of the linear polarizer angle. In addition, to avoid

oxidation of the molecular dyes, the LC microlasers were pumped only in discrete periods of ~200 ms during a spectral scanning process of the CCD.

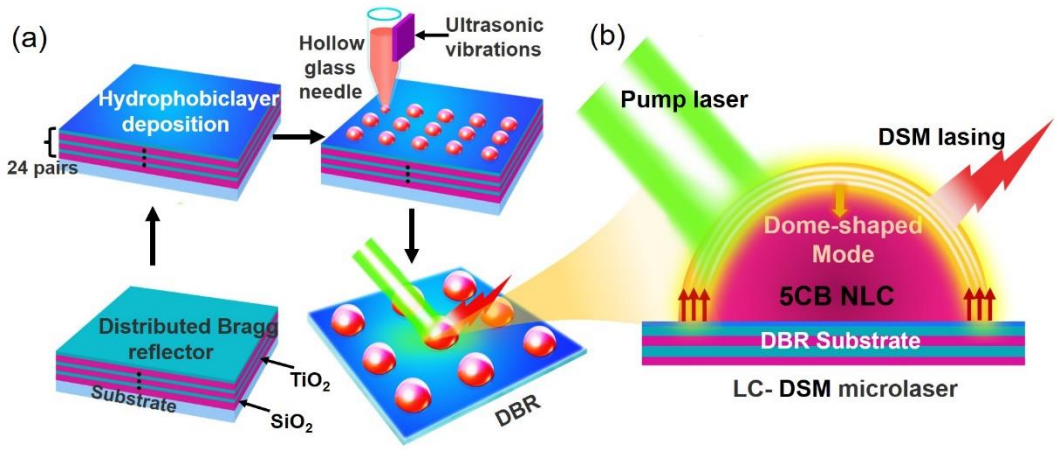

Figure S1. Design and fabrication of LC-DSM microlaser arrays. a) Schematic illustration of the mass production of uniform hemispherical LC droplets on top of DBR substrate via inkjet-printing technique. b) Schematic diagram of the individual LC-DSM resonator. The combination of the total internal reflection on the surface of the light and the strong vertical reflection from the DBR substrate finally forms the DSMs.

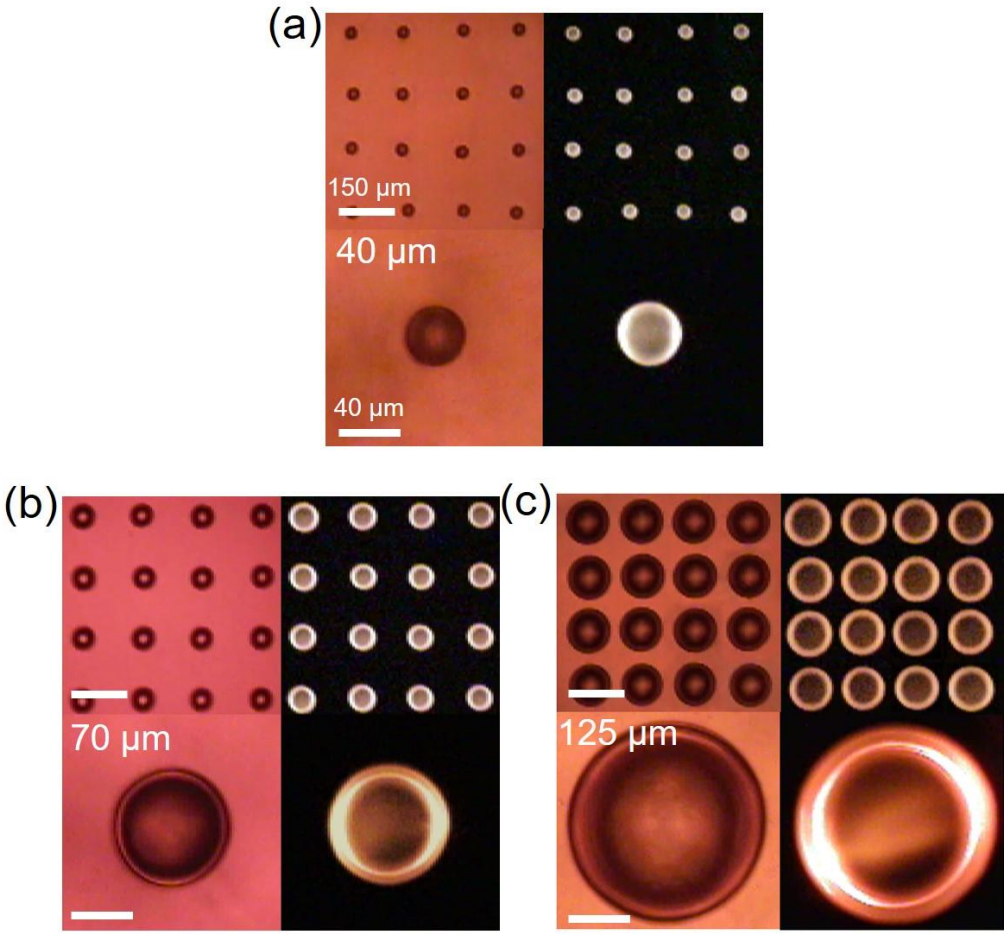

Figure S2. Bright-field microscopy and the corresponding fluorescent image of LC microcavity arrays (top) and the respective single resonator (bottom). The dimensions of (a), (b), (c) three series of LC microcavity arrays are 40 μm, 70 μm, and 125 μm, respectively. Bright spots appeared on both sides of the spherical cap under the excitation of 532 nm pulsed laser.

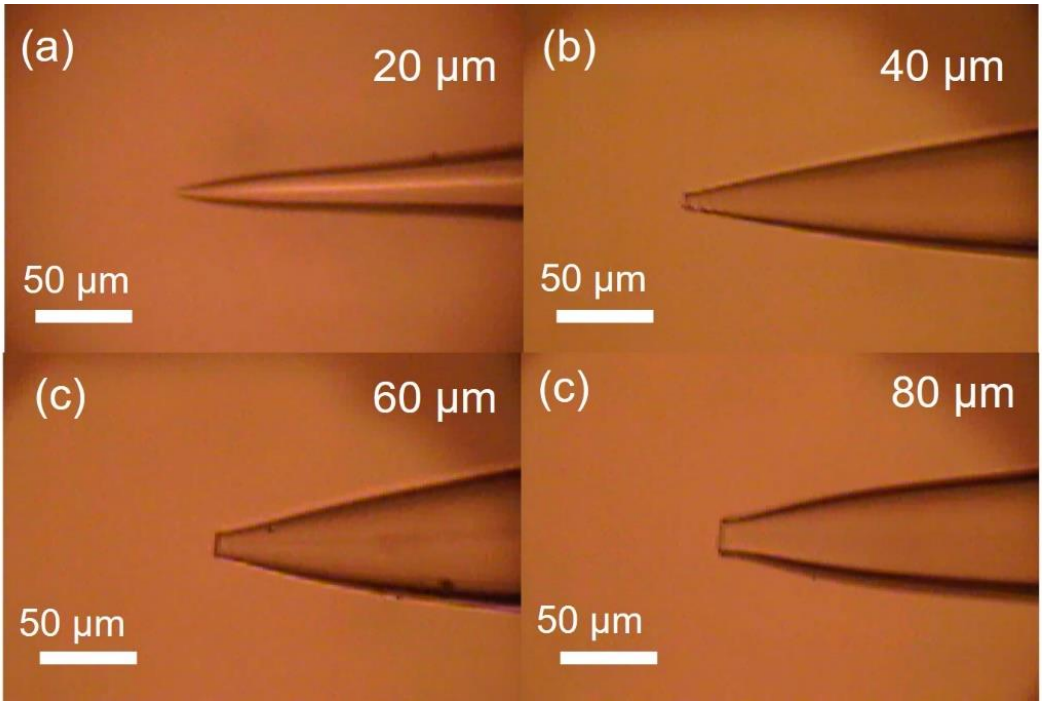

Figure S3. Optical microscope photographs of glass needles with different diameters of (a) 20 μm, (b) 40 μm, (c) 60 μm, (d) 80 μm.

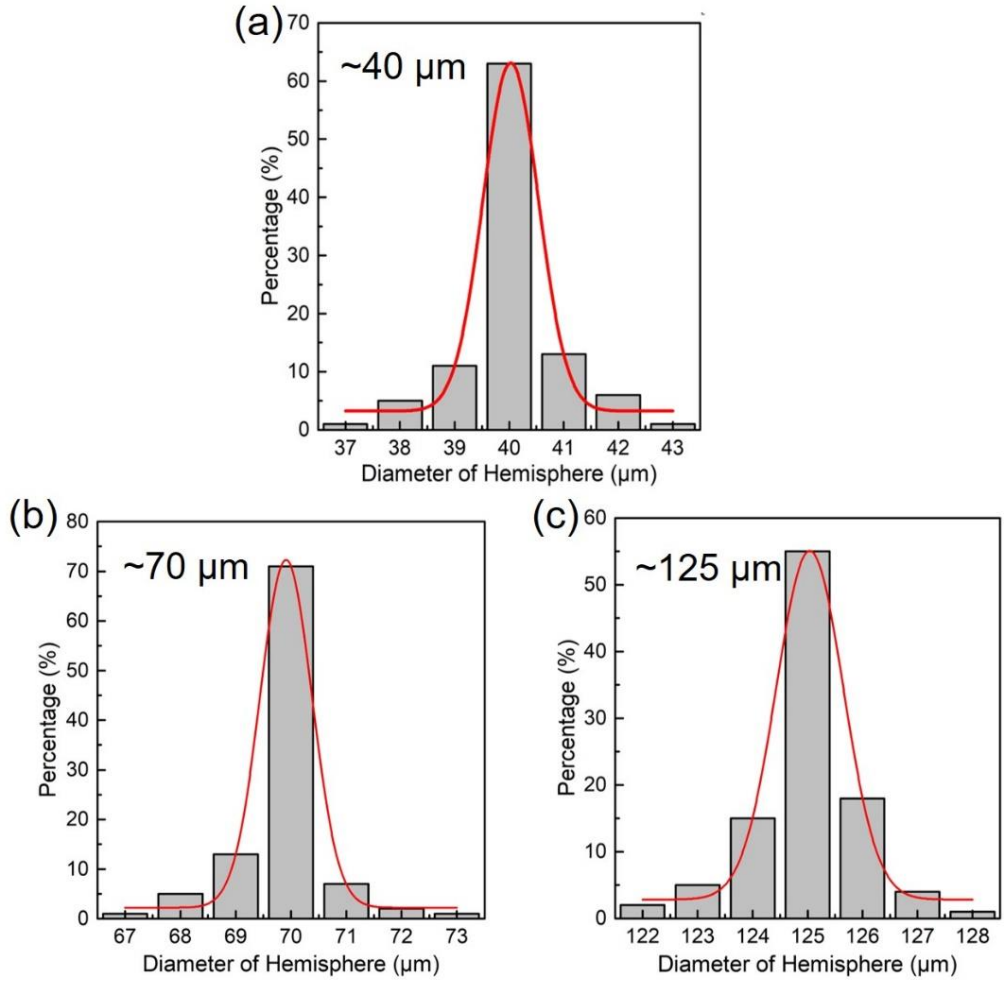

Figure S4. Size distributions of LC-DSM microcavity printed with glass needles of different tip diameters: (a) 40 μm, (b) 60 μm and (c) 80 μm. The average sizes of the three LC cavity arrays are 40.1 (SD ±0.72), 69.7 (SD ±0.69) and 124.6 (SD ±0.91) μm by measuring a total of 192 microcavities, respectively. The distribution can be fairly fitted by a Gaussian curve.

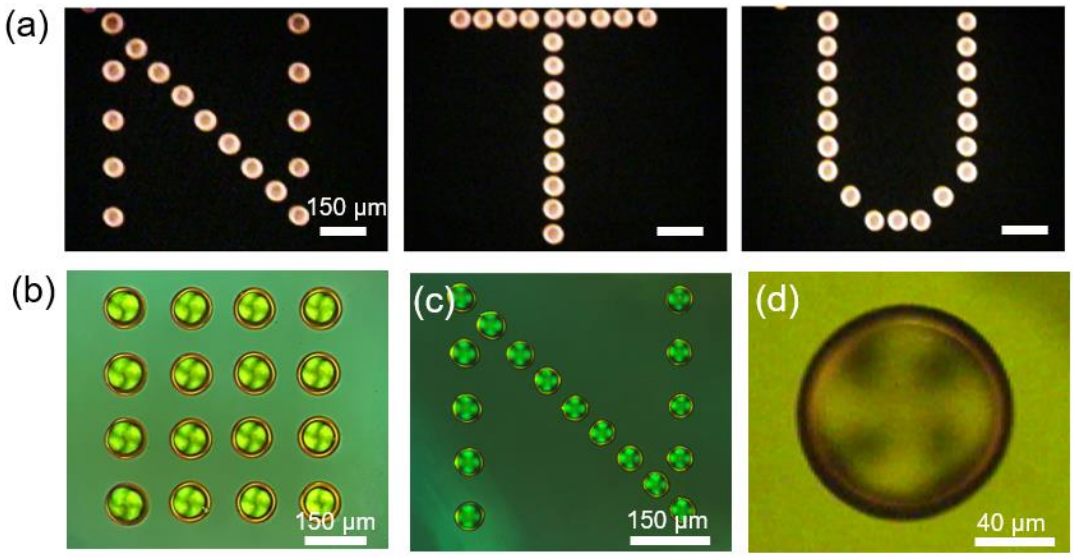

Figure S5. (a) Demonstration of the application of LC-DSM microcavity arrays in "NTU" patterned laser display. (b-d) Polarized optical microscope images of arrayed and monomeric LC microdroplets.

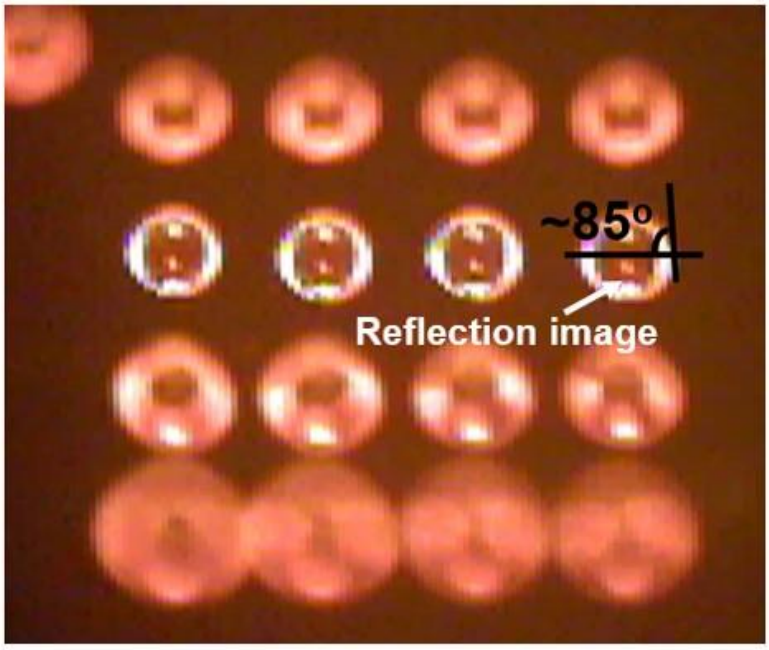

Figure S6. Side-view profiles of the LC microdroplets on the DBR substrate after hydrophobic treatment. The contact angle of substrate was determined to be 85°. This hydrophobic effect is the main drive to the formation of the spherical cap morphology of each droplet.

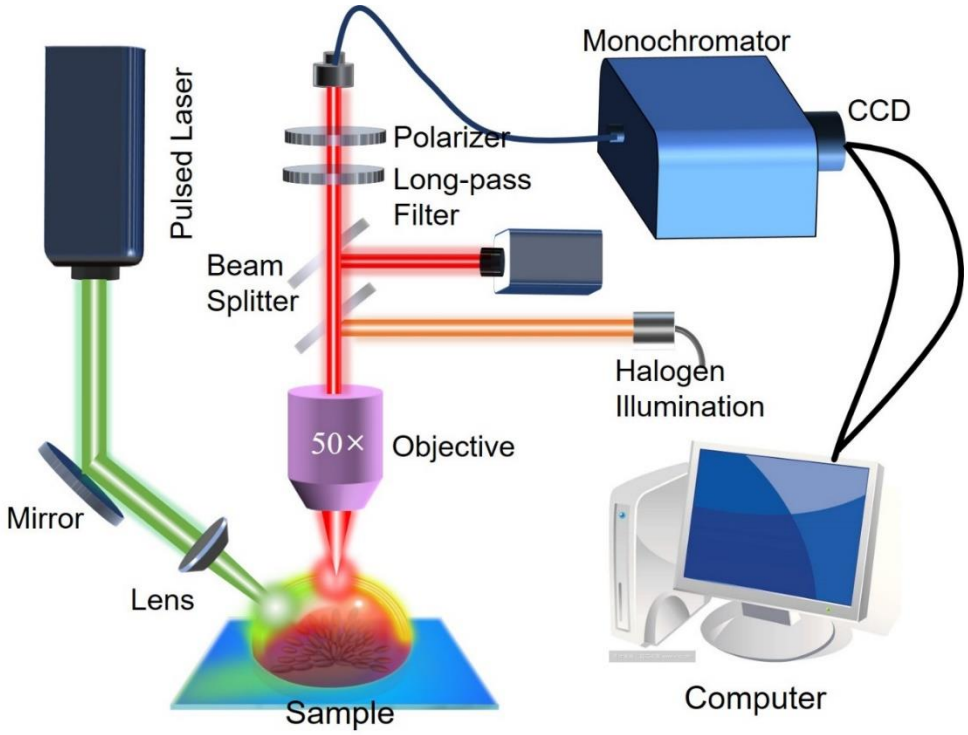

Figure S7. Schematic illustration of the experimental setup for the optical characterization.

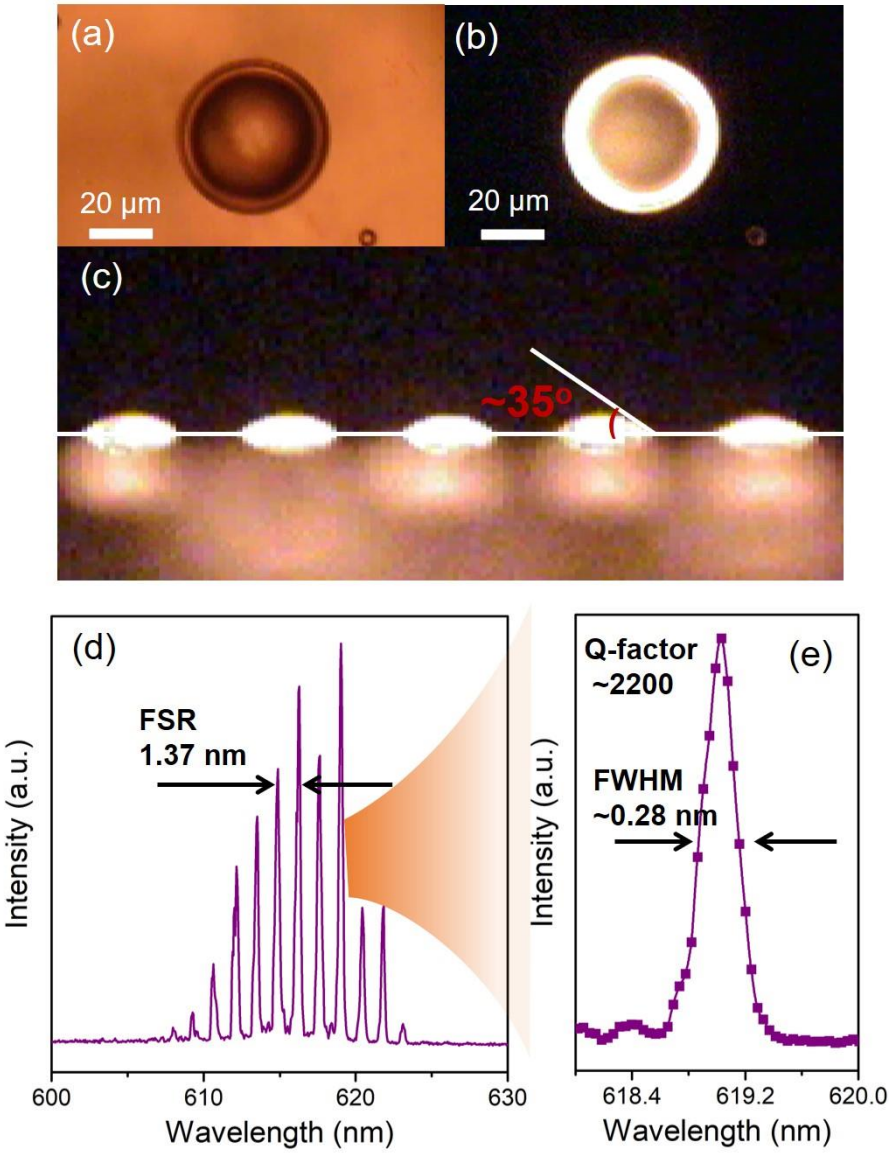

Figure S8. (a) Optical microscope photograph of a LC droplet with a diameter of ~50 μm. (b) Corresponding PL image under 532 nm ns pulsed laser excitation. A bright ring around the LC droplet is an obvious sign of WGMs. (c) Side-view profiles of the LC droplets on the DBR. The contact angle of substrate was determined to be 35°. Typical emission spectrum from an LC-WGM microlaser with a diameter of ~50 μm. The FWHM of lasing single is 0.28 nm, and the lasing Q-factor is ~2200.

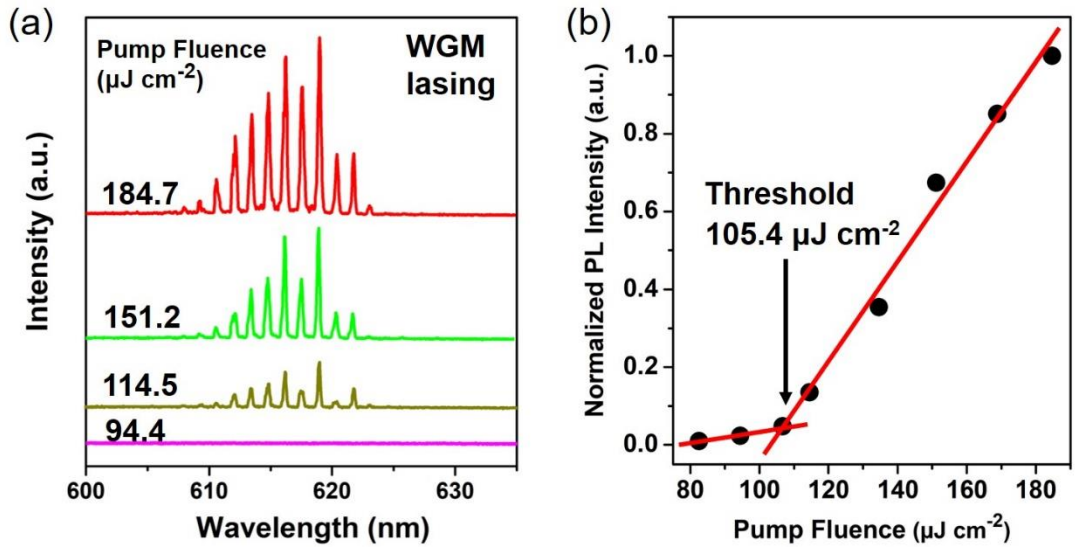

Figure S9. (a) The power-dependent PL spectra of individual LC microlasers with a bottom diameter of ~50 μm. (b) Evolution of the normalized PL intensity of emission peaks as a function of different pump fluence.

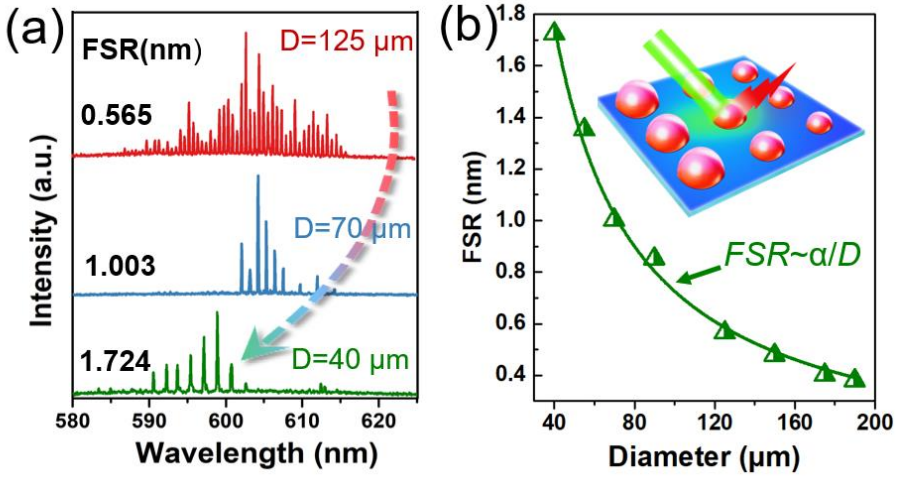

Figure S10. (a) Lasing spectra from LC-DSM microlasers with contact angles α=85° and diameters of 40, 70, and 125 μm, respectively. (b) The FSRs as a function of microlasers' diameter.

In DSMs with a contact angle α=85°, the oscillation path L of the circulating light can be approximated as,

$$L = \pi \frac{\alpha}{180^{\circ}} \frac{2D}{\sin\alpha} \tag{1}$$

here D is the bottom diameter of the microcavity. The free spectral range (FSR) of microlasers with different sizes can be calculated as,

$$FSR = \frac{\lambda^2}{nL} \tag{2}$$

where λ is the resonant wavelength and n is the refractive index of 5CB LC. In our case, the contact angle α=85°, and the cavity bottom diameter D = 40, 70, 125 μm. As shown in **Figure S**10(a), the *FSRs* of the three LC-DSM microlasers with different bottom diameters are 1.724 nm, 1.003 nm, and 0.565 nm, respectively. The corresponding theoretically calculated *FSRs* are 1.750 nm, 1.024 nm, and 0.574 nm, respectively. The good agreement between the theoretical and experimental results of *FSRs* verifies the mechanism of DSM. Moreover, the inverse dependence of *FSR* on *D* also unambiguously validates the DSM properties **Figure S**10(b).

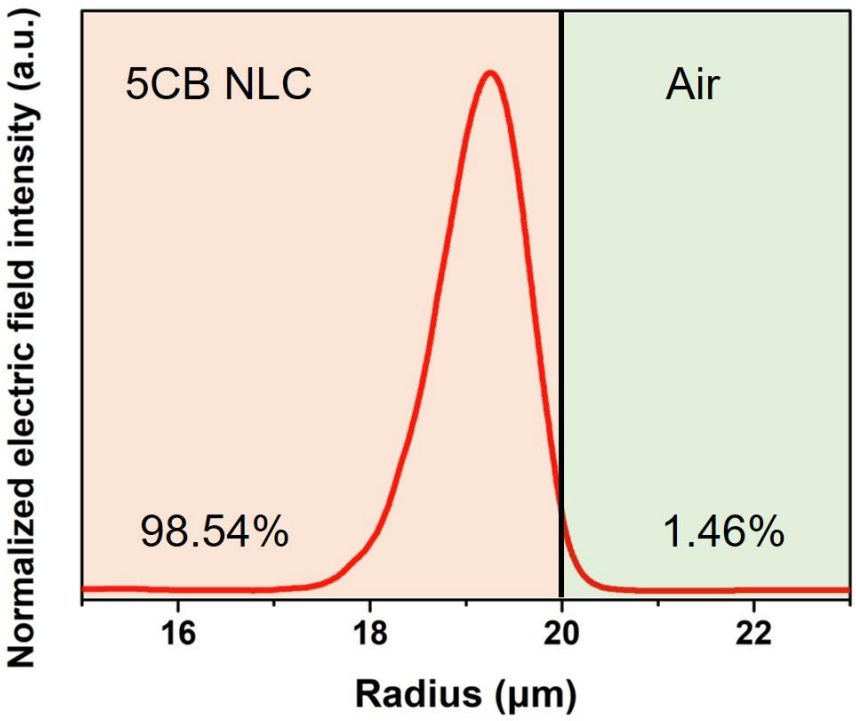

Figure S11. The distribution of normalized DSM electric field |E| intensity. Most all the light field is effectively confined inside the cavity, and only few parts (1.46%) are radiated to the outside in the form of evanescent field.

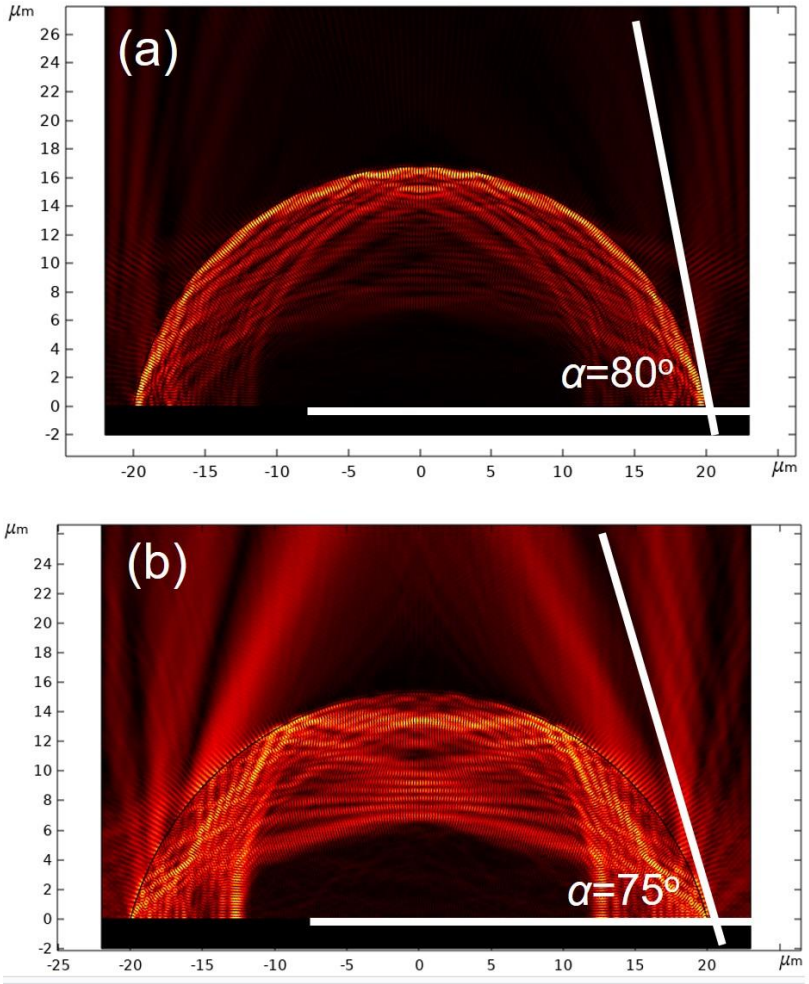

Figure S12. Simulated electric field distribution of the DSMs in LC microcavity with different contact angles of (a) α=80° and (b) α=75°. A large contact angle is an important guarantee for maintaining a high-Q resonant cavity, and a small contact angle will induce the reflection angle of part of the light to be smaller than the critical angle of total reflection, thereby increasing the light loss.

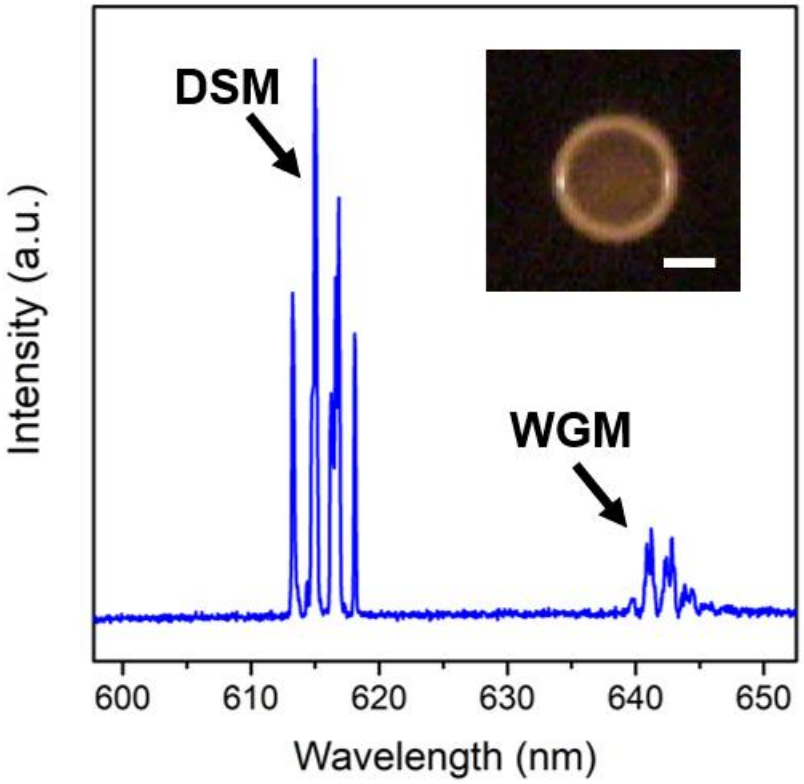

Figure S13. Lasing spectra of a LC microdroplet with a contact angle ~70º. DSM and WGM are observed simultaneously. Scale bar 20 μm.

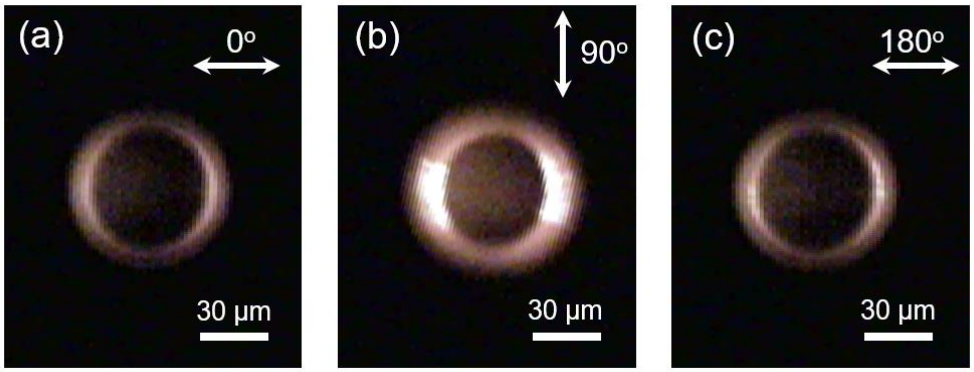

Figure S14. Optical images of the LC-DSM microlaser filtered by the polarizer with polarization directions of 0°, 90°, and 180°.

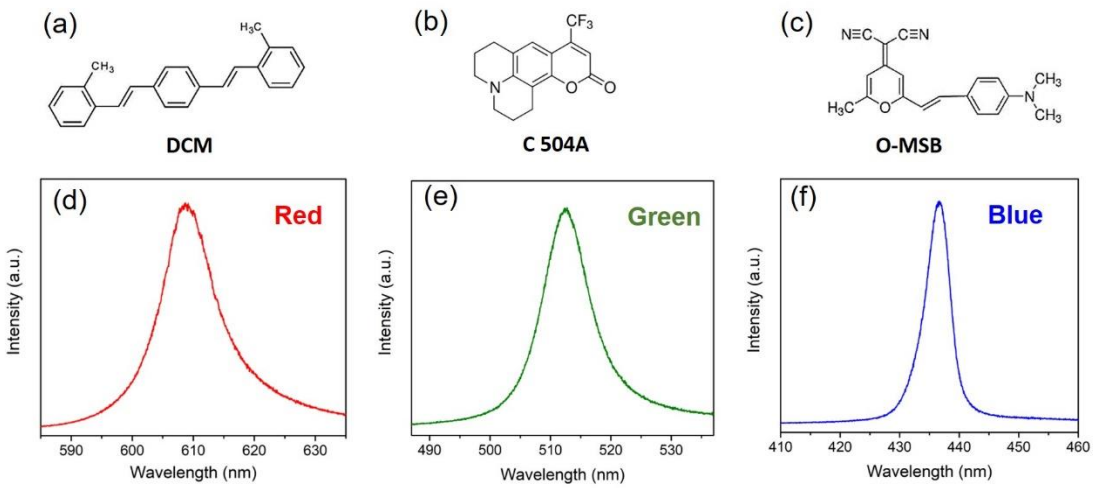

Figure S15. Molecular structures and PL spectra of the three laser dyes in LC. (a-c) Molecular structures of DCM, C 504A, and O-MSB respectively. (d-f) Correspondingly normalized PL spectra for the three dyes in LC.

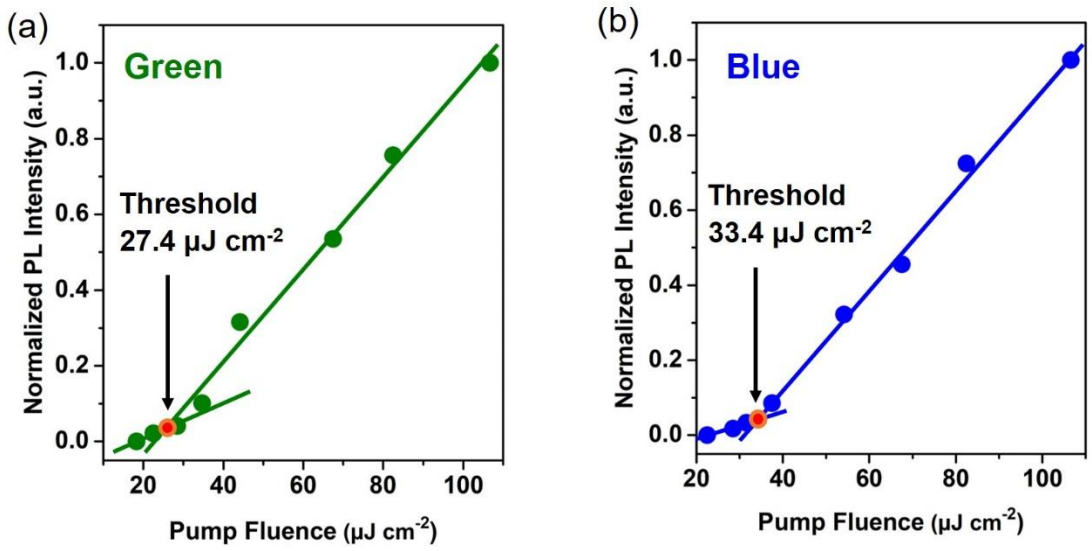

Figure S16. (a) Evolution of the normalized PL intensity of emission peaks as a function of different pump fluence for green LC-DSM microlasers. The lasing threshold was determined to be 27.4 μJ/cm^2. (b) Evolution of the normalized PL intensity of emission peaks as a function of different pump fluence for blue LC-DSM microlasers. The lasing threshold was determined to be 33.4 μJ/cm^2.

Table S1. Lasing features of soft-matter microlasers.

Lasing Type	Materials/Gain	Lasing Threshold	Q-factor	External Environment	Reference
Band-edge lasing	CLC/DCM	~1.5mJ cm^{-2}	~6000	Aqueous solution	[1]
WGM lasing	NLC/DCM	~800 μJ cm^{-2}	~3000	Aqueous solution	[2]
WGM lasing	CLC/NR	~0.5 mJ cm^{-2}	Unknown	Aqueous solution	[3]
WGM lasing	Epoxy resin /R6G	~83 μJ cm^{-2}	~8000	Air	[4]
WGM lasing	Epoxy resin/ Rh B	~2.5mJ cm^{-2}	~5000	Air	[5]
ALM lasing	Water and Glycerol /FITC	~9 mJ cm^{-2}	~3000-5000	Air	[6]
DSM lasing	NLC/DCM	~18.8 μJ cm^{-2}	~24000	Air	*Our work*

[a)] CLC, Cholesteric liquid crystal; NLC, Nematic liquid crystal; NR, Nile Red; Rh B, Rhodamine B; R6G, Rhodamine 6G; PDMS, Polydimethylsiloxane.

Table S2 CIE1931 chromaticity coordinates of the RGB pixel and standard RGB

Sample		Chromaticity coordinates in CIE1931	
		x	y
RGB pixel	R	0.648	0.351
	G	0.155	0.806
	B	0.164	0.011
sRGB	R	0.640	0.330
	G	0.300	0.600
	B	0.150	0.060

References

[1] M. Humar, I. Musevic, *Opt. Express* **2010**, *18*, 26995.

[2] R. Duan,Y. Z. Li, B. J. Shi, H. Y. Li, J. Yang, *Opt. Express* **2019**, *27*, 35427.

[3] C. L. Wang, C. Y. Gong, Y. F. Zhang, Z. Qiao, Z. Y. Yuan, Y. Gong, G. E. Chang, W. C. Tu, Y. C. Chen, *ACS Nano* **2021**, *15*, 11126.

[4] V. D. Ta, R. Chen, H. D. Sun, *Adv. Mater.* **2012**, *24*, OP60.

[5] Ta, V. D. S. C. Yang, Y. Wang, Y. Gao, T. C. He, R. Chen, H. V. Demir, H. D. Sun, *Appl. Phys. Lett.* **2015**, *107*, 221103.

[6] Z. Qiao, X. R. Gong, P. Guan, Z. Y. Yuan, S. L. Feng, Y. Y. Zhang, M. H. Kim, G. E. Chang, Y. C. Chen, *Adv. Photonics* **2021**, *3*, 016003.